Backbone Dynamics of Azurin in Solution: Slow Conformational Change Associated with Deprotonation of Histidine 35[†]

Arnout P. Kalverda,[‡,§] Marcellus Ubbink,*[,‡] Gianfranco Gilardi,[‡,||] Sybren S. Wijmenga,[⊥] Arthur Crawford,[∇] Lars J. C. Jeuken,[‡] and Gerard W. Canters[‡]

Leiden Institute of Chemistry, Leiden University, Gorlaeus Laboratories, P.O. Box 9502, 2300 RA, Leiden, The Netherlands, Nijmegen SON Research Center, Laboratory of Biophysical Chemistry, University of Nijmegen, Toernooiveld, 6525 ED Nijmegen, The Netherlands, and Department of Biochemistry, University of Cambridge, Cambridge CB2 1QW, United Kingdom

ABSTRACT: [15]N relaxation measurements have been performed on the type I blue copper protein azurin from *Pseudomonas aeruginosa*. The relaxation times show that one loop (residues 103−108) and one turn (residues 74−77) display fast internal motions. The rest of the protein is rigid with an average order parameter S^2 of 0.85 ± 0.05. The copper binding site shows the same degree of rigidity even though is it composed of several loops and lies outside the β-sheet sandwich. Substantial exchange broadening was found for a number of residues surrounding the side chain of His-35. The average exchange rate has been determined from NMR exchange spectroscopy experiments and is 45 ± 6 s^{−1} at 41 °C. The exchange broadening is caused by the protonation/deprotonation equilibrium of His-35. The NMR results indicate that the two structures of azurin observed by X-ray diffraction of crystals at pH 5.5 and 9.0 [Nar, H., Messerschmidt, A., Huber, R., Van de Kamp, M., Canters, G. W. (1991) *J. Mol. Biol. 221*, 765−772] are present in solution and that they interconvert slowly.

The type I blue copper protein azurin from *Pseudomonas aeruginosa* is structurally well characterized. Crystal structures have been solved of the protein in the oxidized state at pH 5.5 and 9.0 (*1, 2*), of the apo form (*3*), and of azurin substituted with Zn (*4*), Ni (*5*), and Co (*6*). Furthermore, crystal structures have been reported for numerous site-specific mutants of the protein (*7−16*). NMR[1] assignments and a secondary structure in solution have been reported as well for the azurins from *Pseudomonas aeruginosa* (*17*) and from *Alcaligenes denitrificans* (*18*).

In the past two decades *P. aeruginosa* azurin has been the subject of many spectroscopic studies. A slow exchange process connected with the deprotonation/protonation equilibrium of His-35 was found to affect the protein structure as demonstrated by ^{1}H NMR studies (*19−22*). The exchange between the acid and alkaline forms appeared to be slow in comparison with the chemical shift difference. On the basis of this observation the acid−base exchange rate was estimated as $1 < k < 35$ s[−1] at 22 °C, pH* 6.9 (*21*).

The kinetics of the reaction between azurin and cytochrome c_{551} displays biphasic behavior, of which the slower phase is pH-dependent and has a comparable rate to the acid−base exchange rate of His-35 (*23, 24*). It was therefore assumed that the slow phase is caused by a coupling of the electron-transfer event to the uptake or release of a proton at intermediate pH values (*25*). Replacement of His-35 by Leu or Phe results in the loss of the slow phase, which demonstrates that His-35 is responsible for the coupling (*26*). His-35 has an electrostatic interaction with the copper atom, resulting in a pK_a difference between oxidized and reduced azurin for the protonation of this residue (*27, 28*). More information about the nature of the pH-dependent transition in azurin was obtained from the crystallographic studies (*1*). The crystal structures at pH 5.5 and 9.0 show conformational differences in the region around His-35. Specifically, the Pro-36/Gly-37 peptide bond can flip, so that at high pH a hydrogen bond is formed between Gly-37 HN and His-35

* Address correspondence to this author: Tel (+31-)71-5274628; Fax (+31-)71-5274593; E-mail m.ubbink@chem.leidenuniv.nl.

‡ Leiden University.

§ Present address: Faculty of Biological Sciences, University of Leeds, Leeds LS2 9JT, United Kingdom.

|| Present address: Department of Biochemistry, Imperial College of Science, Technology and Medicine, London SW7 2AZ, United Kingdom.

⊥ University of Nijmegen. Present address: Department of Medical Biochemistry and Biophysics, University of Umeå, S-90187, Umeå, Sweden.

∇ University of Cambridge. Present address: Oxford Molecular Group, Oxford Science Park, Oxford OX4 4GA, England.

[1] Abbreviations: CPMG, Carr−Purcell−Meiboom−Gill; EXSY, exchange spectroscopy; HMQC, heteronuclear multiple quantum coherence; HSQC, heteronuclear single quantum coherence; NMR, nuclear magnetic resonance; NOE, nuclear Overhauser enhancement; ROESY, rotating-frame Overhauser enhancement spectroscopy; S^2, order parameter; SSE, sum of squared errors; T_1, spin−lattice relaxation time; T_2, spin−spin relaxation time; TPPI, time-proportional phase increments; τ_e, effective correlation time describing rapid internal motion; τ_r, overall molecular rotational correlation time.

$N^{\delta 1}$, while at low pH a hydrogen bond is present between the carbonyl oxygen of Pro-36 and the $N^{\delta 1}H$ in the protonated histidine.

The dynamical behavior described above constitutes an interesting contrast with the notion of an essentially rigid environment that is imposed by the protein on the metal. Such rigidity is thought to be important for electron transfer by minimizing the reorganization energy for electron transfer. The idea of a relatively rigid Cu site has been supported by the observation of low crystallographic *B*-factors in the region around the metal, the observation of many hydrogen-bonding interactions in the active-site region (*29*), slow hydrogen exchange observed for a number of amide protons in the Cu ligand-bearing loops (*17*), and finally, the small conformational differences between the crystal structures of apoazurins and metal-substituted azurins and the native, Cu-containing proteins.

A more quantitative picture of the dynamical features of the azurin molecule, its Cu-site environment, and the His-35 region can be obtained by utilizing ^{15}N relaxation measurements. Dynamical features of the protein play a role in such processes as the uptake of copper by the apoprotein, as hinted at in a crystallographic study of apoazurin (*3*), which shows the presence of two conformers of His-117, one of the Cu ligands in the holoprotein. Other dynamical processes may be related to the fine-tuning of the redox potential by pH-dependent conformational changes. Examples are the protonation of ligand His residues in amicyanins and plastocyanins (*30, 31*) and the His-35 protonation in *P. aeruginosa* azurin, albeit the physiological significance of these effects has not been clarified.

In the present study the dynamic properties of azurin in solution have been analyzed by studying ^{15}N relaxation. The protein is highly rigid, with fast internal motions only in two of the loops that connect the β-strands. The copper binding site, which is formed by four loops, shows the same rigidity as the core of the protein. The conformational dynamics of the His-35 side chain shows a marked influence on the ^{15}N T_2 relaxation times of the amide nitrogens in its vicinity.

EXPERIMENTAL PROCEDURES

Sample Preparation. Preparation and purification of ^{15}N-labeled azurin was performed as described previously (*17*). Samples for NMR contained 2 mM azurin in 20 mM potassium phosphate, pH 5.5, in 90% H_2O/10% D_2O. To prepare Cu(I) azurin, a solution of oxidized azurin was deoxygenated in the NMR tube by a repeated cycle of evacuation and argon flushing in a closed system. Reduction of the metal center was achieved by adding sodium dithionite (0.1 M in 0.1 M NaOH) after which the argon treatment was repeated once more. The tube was closed with a rubber cap. Prepared in this way, azurin stayed reduced for at least 2 months.

NMR Spectroscopy. NMR experiments were performed at 41 °C on an AMX 600 MHz Bruker spectrometer. ^{15}N spin−lattice relaxation time constants (T_1), spin−spin relaxation time constants (T_2), and {^{1}H}−^{15}N NOEs were measured with the pulse sequences described by Barbato et al. (*32*). ^{1}H-detected ^{15}N T_1 experiments were recorded with 128 t_1 increments and 1K complex t_2 points. Thirty-two scans were acquired per t_1 point. The spectral widths used were 2.5 kHz

(^{15}N, F_1) and 10 kHz (^{1}H, F_2). Ten experiments were recorded, each with a different value for the longitudinal relaxation period (20, 41, 69, 97, 153, 238, 336, 462, 687, and 912 ms) to obtain the ^{15}N T_1 relaxation rates. The relaxation delay between scans was 1.5 s. ^{15}N T_2 experiments were recorded with 256 t_1 increments. Twenty-four scans were acquired per t_1 point. Ten experiments were recorded with different values for the duration of the CPMG sequence (8.3, 33.3, 58.2, 83.2, 116.5, 149.8, 183.0, 216.3, 249.6, and 291.2 ms). The delay between 180° pulses in the CPMG sequence was set to 1 ms. A recycle delay of 1.5 s was used between scans. Two spectra were collected for the measurement of the ^{1}H−^{15}N NOE, one with proton saturation and one without; a recycle delay of 4 s was used. The experiments were recorded with 256 t_1 increments of 96 scans. Saturation of the ^{1}H spectrum was achieved by applying nonselective 120° pulses every 20 ms during the recycle delay. The solvent signal was suppressed with a 5 ms trim pulse preceding the preparation pulse. The spectral widths used were 2.5 kHz (^{15}N, F_1) and 10 kHz (^{1}H, F_2). A total of 1K complex data points were collected in F_2. The ^{1}H carrier was positioned on the H_2O resonance and the ^{15}N carrier was positioned at 119 ppm. Quadrature in the F_1 dimension was obtained by use of TPPI.

Data sets were processed by using the NMRi software (New Methods Research, Syracuse, NY). Cosine bell apodization was applied to both dimensions, and zero-filling was used to obtain a size of 1024 × 2048 real data points in Fourier-transformed spectra. Baseline corrections were applied by use of FLATT (*33*). Resonance intensities were determined with the peak-picking routine in NMR2.

Two-dimensional HMQC spectra with a jump−return water suppression were recorded at pH values of 6.3, 6.6, 6.8, 7.2, and 7.6. To further describe the slow pH-dependent conformational exchange equilibrium, the following NMR experiments were also conducted with a 2 mM sample of nonlabeled azurin at pH 7.0: a 2D ROESY with a 50 ms mixing time and a series of EXSY spectra with mixing times of 20, 40, 60, 80, 110, and 150 ms.

Analysis of Relaxation Data. ^{15}N T_1 and ^{15}N T_2 relaxation times were obtained by fitting of the peak intensities to a monoexponential decay. The standard errors in the fitted parameters were determined from the scatter of the data points around the fitted exponential curve. They ranged from 1% to 6% for the ^{15}N T_1, with the exceptions of F114 (12%) and N18 (7%), and were between 2% and 5% for the ^{15}N T_2 fitting. The steady-state NOE was calculated as the ratio of the peak heights in the spectra recorded with and without proton saturation. The error in the peak intensities was estimated from the baseplane noise by taking the average of the largest noise intensities encountered in a number of baseplane regions.

The relaxation data were analyzed by a computational data fitting based on the model-free approach of Lipari and Szabo (*34, 35*). The use of this approach for the analysis of ^{15}N relaxation data is similar to that adopted by several other authors (*36−38*). The spectral density function $J(\omega)$ is modeled as

$$J(\omega) = \frac{2}{5}\left[\frac{S^2\tau_r}{1 + (\omega\tau_r)^2} + \frac{(1 - S^2)\tau}{1 + (\omega\tau)^2}\right] \quad (1)$$

where τ_r is the correlation time for overall tumbling of the molecule, S^2 is the generalized order parameter characterizing the amplitude of internal motions, and $\tau^{-1} = \tau_r^{-1} + \tau_e^{-1}$, in which τ_e is the correlation time for internal motion. When the internal motion is very fast ($\tau_e < 10$ ps), the spectral density function simplifies to

$$J(\omega) = \frac{2}{5}\left[\frac{S^2\tau_r}{1 + (\omega\tau_r)^2}\right] \qquad (2)$$

The T_1, T_2, and heteronuclear NOE depend on the spectral density at five characteristic frequencies. The model for $J(\omega)$ (eq 1 or 2) can be used to fit the experimental relaxation data with the model-free parameters S^2, τ_r, and τ_e. In addition, the T_2 relaxation may be affected by conformational exchange, causing a significant shortening of the T_2 values. If this is the case, an additional parameter (R_{ex}) has to be included, describing the exchange contributions to the T_2 relaxation, defined as the excess line width due to the exchange process. All in all there are four adjustable parameters in the model. One of these, the overall rotational correlation time τ_r, is the same for all residues under the assumption of overall isotropic molecular tumbling of the protein and can be estimated from the average T_1/T_2 ratio (*37*). In principle, this leaves three parameters that have to be adjusted for each residue.

Since there are only three experimental values per residue, some care has to be exercised as to how many parameters need to be included for each residue to produce a satisfactory fit. The relaxation data were fitted with three dynamical models: (1) the simplified spectral density function (eq 2), (2) the simplified spectral density function combined with R_{ex}, and (3) the more complicated version of the spectral density function including both S^2 and τ_e (eq 1). In this way, at most two parameters were adjusted for each residue (S^2, S^2 and R_{ex}, or S^2 and τ_e, respectively).

An initial estimation of the overall molecular correlation time was based upon the average T_1/T_2 ratio. Under conditions where $\tau_e < 100$ ps and in the absence of exchange broadening this ratio is essentially independent of S^2 and τ_e (*36*). The average T_1/T_2 ratio was calculated with exclusion of the 10% most extreme values, leading to a trimmed average ratio of 3.36 (± 0.23). The correlation time for overall molecular tumbling was then initially estimated as $\tau_r = 5.0$ (± 0.5) ns. With this value of τ_r, the T_1, T_2, and NOE were fitted to all three models with the software package Modelfree 4.0 (*38, 39*; available at http://cpmcnet.columbia.edu/dept/gsas/biochem/labs/palmer/#sftwr). If the sum of squared errors (SSE), as defined in the manual of Modelfree 4.0, was >10 for model 1, models 2 or 3 were used, provided that they gave a lower SSE. For most residues, SSE = 10 agreed approximately with a 5% confidence level for the appropriateness of the used model. After selection of the models, τ_r was optimized (4.7 ns) and the final S^2, R_{ex}, and τ_e values were calculated with the optimized τ_r. Standard deviations for the fitted parameters were obtained from a Monte Carlo simulation procedure. Three hundred minimizations were performed with data simulated around the mean experimental values, according to a Gaussian distribution with the experimental errors taken as the standard deviation of this distribution.
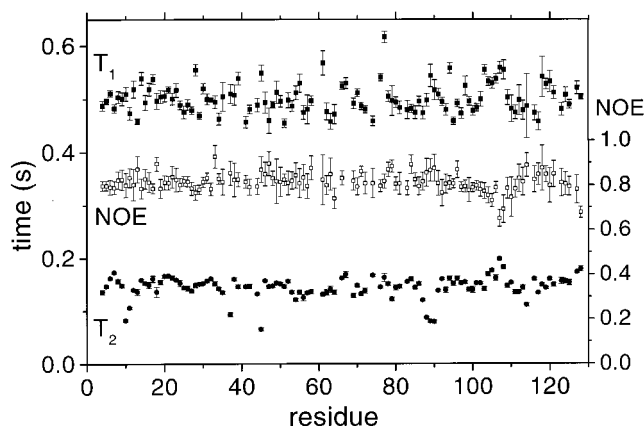

FIGURE 1: Relaxation data for azurin. Relaxation data measured for the individual amides are plotted against the residue number: (■) ^{15}N T_1; (●) ^{15}N T_2; (□) ^{1}H$-^{15}$N NOE.

No attempt was made to introduce both τ_e and R_{ex}, since the amount of experimental data available does not warrant such an analysis. In principle, it is possible to extend the amount of experimental data by measuring other relaxation parameters or by repeating the relaxation measurements at different magnetic fields (*40, 41*), but this approach was not adopted since the present data allow for a consistent analysis.

RESULTS

Relaxation Data. Out of 123 backbone amide groups in azurin, 113 were sufficiently resolved to obtain ^{15}N T_1 and T_2 values. The peaks with the shortest ^{15}N T_1 or T_2 relaxation periods had signal-to-noise ratios of 25–50. The T_1 and T_2 relaxation times were obtained from monoexponential fitting of the peak height data. The T_1, T_2, and NOE values are presented in Figure 1.

The values of the heteronuclear NOE provide a qualitative description of the extent of fast internal motions in the molecule. The average NOE value is 0.82 (± 0.04), which corresponds with the value expected in the absence of internal motions on a time scale faster than the molecular tumbling. Four residues have NOE values that are lower than average by more than 2 standard deviations: 105, 107, 108, and the C-terminal residue 128, the lowest value being 0.65 for Gln-107, showing that the loop encompassing residues 105–108 has considerable internal motion. The absence of negative NOE values indicates that there are, however, no unordered backbone amide groups in the molecule. A number of NOEs lie in the range 0.85–0.93. This may arise because the peak intensity in the experiment recorded without proton saturation for fast-exchanging amides can be reduced relative to its true value due to incomplete equilibration of the ^{15}N and ^{1}H magnetization during the relaxation delay of the experiment as a result of the amide exchange (*36, 37, 42, 43*).

Most of the T_1 values lie in the range 0.45–0.52 s, the average value being 0.50 (± 0.02) s (see Figure 1). Eleven residues have T_1 values higher than 0.54 s (residues 28, 45, 61, 76, 77, 89, 94, 103, 107, 108, and 118). There are also a number of amide groups with T_1 values between 0.52 and 0.54 s. Noteworthy is Asp-77, which has by far the largest T_1 value of 0.617 s.

The T_2 values cover a large range: from 65 ms for Gly-45 up to 198 ms for Gln-107 (see Figure 1). The majority of the values are in the range 130–170 ms. Diagnostic of
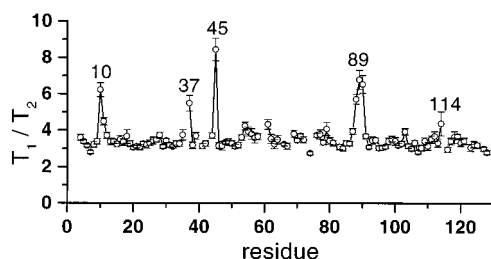
FIGURE 2: T_1/T_2 ratio, plotted against the residue number. Some residue numbers are shown in the plot.

Table 1: Relaxation Parameters for Trp 48 $N^{\epsilon 1}$

T_1 (s)	T_2 (s)	NOE	$S^{2\ a}$
0.57 ± 0.01	0.171 ± 0.006	0.76 ± 0.04	0.89 ± 0.02

^{a} The order parameter is calculated from the relaxation data by using a chemical shift anisotropy of -89 ppm (*57*).

the motional properties of the molecule are a group of residues with significantly longer T_2 values and a group for which the T_2 values are significantly shorter. The first group is formed by residues 7, 105, 107, 108, 127, and 128 with T_2 between 0.17 and 0.20 s, indicative of increased internal motion. The second group, formed by residues 10, 11, 37, 45, 88−90 and 114, has T_2 values that are much shorter than average, which is an indication that they are involved in chemical exchange. These residues also clearly stand out in Figure 2, where the T_1/T_2 ratios are plotted for the backbone amide groups. It is clear that these have an exchange contribution to the T_2 (*37*). Apart from the backbone nitrogens, *P. aeruginosa* azurin harbors a side-chain nitrogen on the single tryptophan residue in the core of the molecule (Trp-48). The relaxation data for the Trp $N^{\epsilon 1}H$ are summarized in Table 1. They indicate that the Trp side chain is just as rigid as the majority of the backbone amides.

Model-Free Calculations. An initial estimation of 5.0 (± 0.5) ns of the overall molecular correlation time (τ_r) was made, based upon the average T_1/T_2 ratio. With this value, order parameters were calculated by use of the three dynamic models mentioned in the Experimental Procedures (defined by the parameters S^2, S^2 and R_{ex}, or S^2 and τ_e, respectively) and the optimized value of $\tau_r = 4.7$ (± 0.1) ns was obtained. The results are presented in Figure 3.

A value of τ_e was optimized for residues 74, 105, 107, 127, and 128. Lys-74 needed a very large value of $\tau_e = 1.3$ (± 0.2) ns. This is an indication that for adequate fitting of this residue a more complicated motional model should be used, since the internal motion seems to be on a time scale comparable to τ_r (*34, 37*). That there are relatively few residues for which inclusion of τ_e has an effect on the order parameter fitting can be expected. Virtually all residues have a heteronuclear NOE > 0.74, indicating that τ_e must be very short. Therefore most of the relaxation data should be accounted for by model 1, with only S^2 as a fitted parameter (see eq 2).

A value for R_{ex} was included in the order parameter fitting for 25 residues. For the majority of these, $R_{ex} < 1.5$ Hz. There are, however, eight residues that require substantially larger values of R_{ex} (2−9.5 Hz). These correspond to the residues with highly increased T_1/T_2 ratios and will be discussed in a later section.
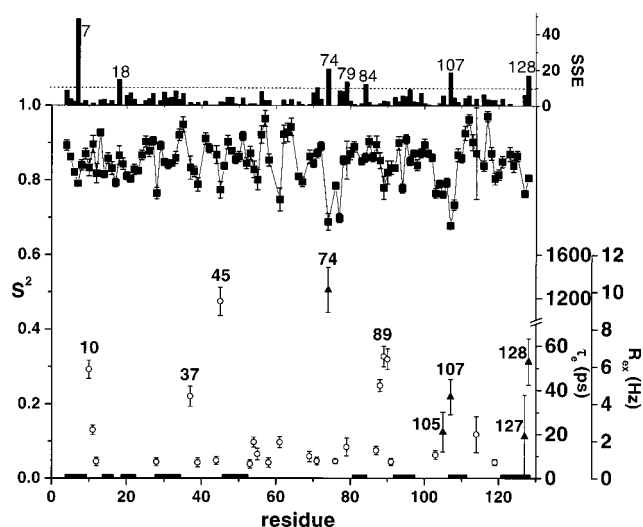

FIGURE 3: Mobility plot of azurin. (■) Order parameters (S^2); (○) exchange contributions to the T_2 (R_{ex}); (▲) correlation time of internal motion (τ_e). Vertical bars represent the sum of squared errors (SSE). The dashed line at SSE = 10 represents approximately a 5% confidence level for the appropriateness of the model used to fit the relaxation data of the residue. Model 1, only S^2; model 2, S^2 and R_{ex}; model 3, S^2 and τ_e. The horizontal bars on the abscissa indicate the positions of the β-strands in azurin.

Seven residues have a final sum of squared errors (SSE, as defined in the Modelfree 4.0 manual) > 10, indicating that none of the models can be considered, with good reliability, to be appropriate to fit the data (see Figure 3). Finally, the data of one residue that also shows an increased T_1/T_2 ratio, Phe-114, could be fitted with model 2 but yielded a large error in S^2. This is a result of the extraordinarily large error in the T_1 value for this residue. The average order parameter is 0.86 (± 0.05). The residues K74, D77, Q107, and Y108 have $S^2 < 0.75$.

Slow Conformational Exchange. At pH values close to the pK_a of His-35, two distinct chemical shift values were observed for the protons and nitrogens in the neighborhood of the histidine ring. On the basis of pH-dependent changes in peak intensities in the jump−return HMQC spectra, the pK_a of His-35 was determined to be 7.0 (± 0.1) in 20 mM potassium phosphate at 41 °C. Exchange peaks between the low- and high-pH form of the protein were detected by recording a 50 ms ^{1}H-ROESY at pH 7.0. To obtain an estimate of the rate of the process, a series of ^{1}H-EXSY spectra was recorded with mixing times ranging from 20 to 150 ms. The cross-peak volumes of 10 exchange cross-peaks originating from five protons (the volumes of the cross-peaks on both sides of the diagonal) were measured. These protons were the $C^{\epsilon 1}H$ of His35 and four amide protons in the immediate environment of the side chain of H35 (residues G9, G37, G88, and E91). The cross-peak volumes were fitted to the equations of Jeener et al. (*44*) for a reversible two-site exchange. The volumes of the cross-peaks, a_{AB} ($=a_{BA}$), connecting forms A and B are given by

$$a_{AB}(\tau_m) = a_{BA}(\tau_m) = ce^{-(r+k)\tau_m} \sinh(k\tau_m) \qquad (3)$$

where r is the intrinsic spin−lattice relaxation rate (assuming $r_A = r_B$), k is the average rate constant for the process [$k = (k_{AB} + k_{BA})/2$], c is a scaling factor, and τ_m is the mixing time. The data for the cross-peaks could be fitted with a
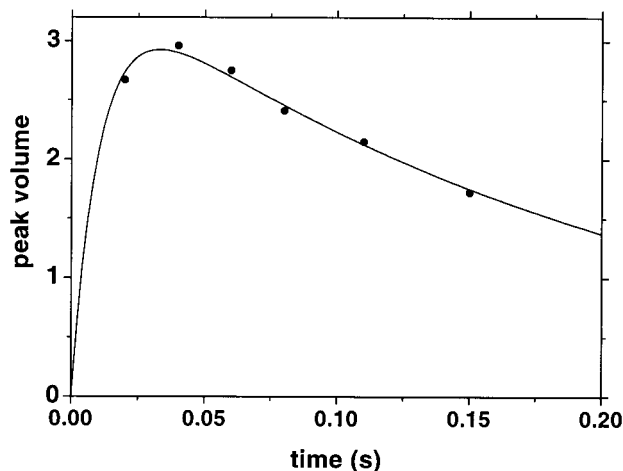
FIGURE 4: Exchange broadening of His-35: Time course of the cross-peak volume of the exchange cross-peak between the low- and high-pH resonance position of His-35 $C^{\epsilon 1}H$. The line indicates the fit to eq 3 with $k = 45$ s^{-1}.

single average exchange rate of $k = 45$ (± 6) s^{-1}. An example is given in Figure 4. The value of r varied between 4 and 8 s^{-1} for the different protons. The value of 45 (± 6) s^{-1} for the exchange rate at 41 °C is only slightly faster than the previous estimate of $1 < k < 35$ s^{-1} that was obtained at 22 °C (24). The exchange rate is derived at the pK_a of the process, so equal populations of both species are present, and thus $k_{AB} = k_{BA} = k$. At this pH, the correlation time τ_{ex} of the exchange process, defined as $1/(k_{AB} + k_{BA})$ or $1/2k$, is 11 ± 2 ms.

Another method to determine the exchange rate is based on the line broadening of the ^{15}N signals. For this method, it is necessary to determine the differences in chemical shift between the signals of the two species. By combining the HMQC spectra at different pH values between 6 and 8 with the cross-peak locations in the ROESY spectrum at pH 7.0, the ^1H and ^{15}N chemical shifts for both the low- and the high-pH form could be found for three amides from which the difference between the ^{15}N chemical shifts in the two forms could be calculated. These chemical shift differences were quite sizable and amounted to 340 Hz for G37 and about 400 Hz for G88 and G90.

The average exchange rate could be calculated on the basis of the transverse relaxation rates of these residues, from the equations describing the effect of chemical exchange on the transversal magnetization decay during a CPMG pulse train (45−47):

$$\Delta_{ex} = \frac{1}{4}\{k - (1/2\tau) \ln [F + (1 + F^2)^{1/2}]\} \qquad (4)$$

For $k < \omega_{ex}$, $F = [\tau k \sin 2u]/u$; for $k = \omega_{ex}$, $F = 2\tau k$; and for $k > \omega_{ex}$, $F = [\tau k \sinh 2u]/u$; $u = \tau|k^2 - \omega_{ex}^2|^{1/2}$. Δ_{ex} is the contribution to the line width due to the chemical exchange process, ω_{ex} is the chemical shift difference between the two forms in radians per second, τ is the spin− echo period in the CPMG sequence, and k again represents the average rate constant [$k = (k_{AB} + k_{BA})/2$]. Equation 4 assumes equal populations of both forms, $p_A = p_B = 0.5$. It can be used to estimate the line broadening in the more general case by substituting $\omega_{ex}^2 = 4p_A p_B \omega'_{ex}^2$, where ω'_{ex} is the true chemical shift difference between the two unequally populated sites (47).
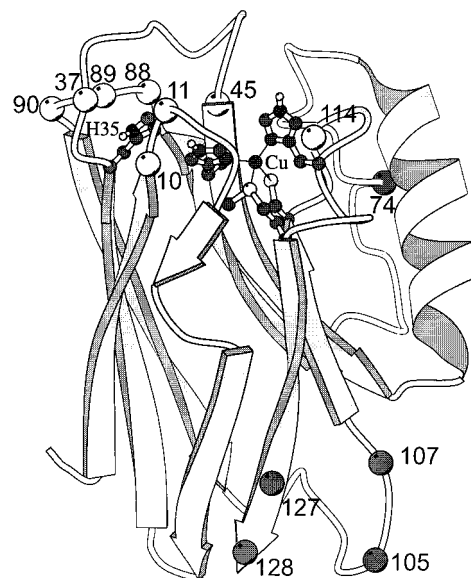

FIGURE 5: Representation of the dynamical behavior of azurin superposed on a structural model of the protein. The side chains of the copper ligands and of His-35 are shown in ball-and-stick representation. The dark spheres at the C^α positions indicate residues with an increased backbone mobility. The light spheres at the C^α positions indicate residues that experience exchange broadening.

Since the ^{15}N T_2 relaxation measurements were performed at a pH of 5.5 and the pK_a of the histidine deprotonation is 7.0 (± 0.1) in H_2O the relative populations of the two forms can be estimated as 0.96−0.98 for the protonated and 0.02− 0.04 for the deprotonated form. With these values, the experimentally observed line broadenings are reproduced for the amides of G37, G88, and G90 with $k = 60$ (± 30) s^{-1}, giving $\tau_{ex} = 8$ (± 4) ms at pH 5.5.

The exchange rates at pH 7.0 and 5.5 agree with a conformational exchange process that is slow on the chemical shift time scale.

DISCUSSION

Increased Backbone Mobility. From the order parameters (Figure 3) and the values of the ^1H−^{15}N NOE (Figure 1), it is apparent that *P. aeruginosa* azurin is a rigid protein, with only limited internal motion of the backbone on a time scale faster than the rate of molecular tumbling for the majority of the protein's amide groups. This behavior is as might be expected for a protein with a very high β-sheet content. Higher mobility, if any, will be restricted to the loops connecting the β-sheets. In Figure 5 the different types of mobility found in the structure are superimposed on a representation of the fold of azurin. Residues that required a τ_e in the modeling of the relaxation data, indicating the presence of fast backbone motions, are represented as dark spheres (74, 105, 107, 127, and 128). Residues that needed an $R_{ex} > 2$ Hz in the order parameter fitting, indicating the presence of chemical exchange on the micro- to millisecond time scale, are represented by light spheres (10, 11, 37, 45, 88−90, and 114).

An increase in both T_1 and T_2 for residues 103−108 shows that this region displays rapid backbone motion, although the decrease in S^2 is only limited, with Gln-107 having the lowest value of S^2 (0.68). This is the only extended region of increased flexibility, which is also manifested in the
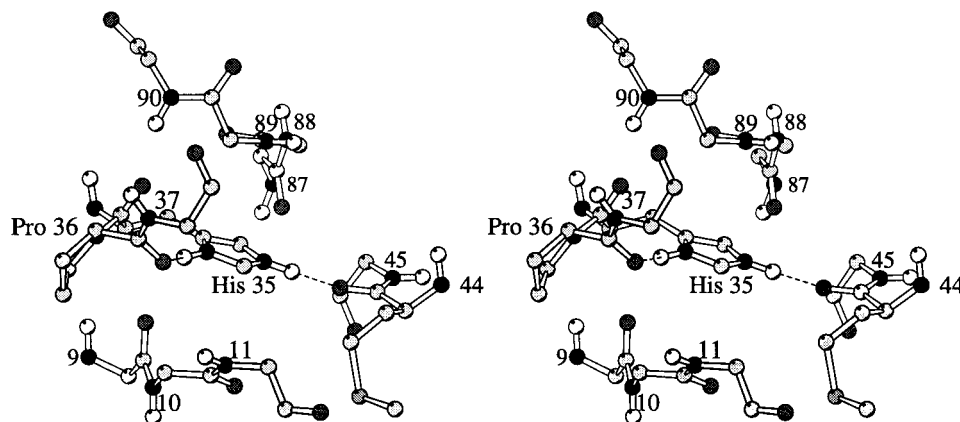
FIGURE 6: Immediate surroundings of the His-35 ring. The dashed lines indicate the hydrogen bonds of the His-35 side chain in the crystal structure at pH 5.5. The white spheres are the amide protons; dark spheres are nitrogen and oxygen atoms. With the exception of the region 35−37, only the backbone is shown. Only protons attached to nitrogens are depicted.

heteronuclear NOE values that are notably smaller in this region. Apart from this long loop there is one other region displaying fast internal motion. The two residues K74 and D77 have S^2 of 0.69 and 0.70, respectively. In the crystal structure of azurin there is a type I turn between K74 and D77. The data presented here suggest that this turn is involved in internal motion. The high value of τ_e for Lys-74 and the high SSE, caused by the poor fit of the NOE, in this region (Figure 3) suggest that this internal motion could be on the intermediate rather than the fast time scale.

With regard to the Cu site, the Cu ligand His-46 and the surrounding residues have values for the relaxation data that are close to average, with the exception of Gly-45 as discussed in the section about conformational exchange. The loop 112−121 bearing the other three ligands shows somewhat more complex behavior. Most outstanding are a low T_2 value of F114 (0.11 s), an exceptionally high S^2 of 0.97 for His-117, and slightly higher T_1 values for residues 118−120. However, the other values of the relaxation parameters are close to average, which lead to the conclusion that the Cu site basically shows the same pattern of rigidity as the core of the molecule.

Comparison with B-Factors. Although there is usually not a close correspondence between ^{15}N relaxation data and *B*-factors, it is interesting to make a comparison between the *B*-factors from the crystal structure determination of *P. aeruginosa* Cu(I) azurin (*48*) and the values of the order parameter. Apart from the C- and N-termini and excluding single residues, there are five regions with *B*-factors > 20 Å^2 in the crystal structure of *P. aeruginosa* azurin. Two of these overlap with the two regions where the relaxation data point to the presence of backbone mobility: the loop (103−108) connecting β-strands 6 and 7 displays increased *B*-factors for the main-chain atoms in both the crystal structures from *P. aeruginosa* and *A. denitrificans* (*29, 47*). Internal flexibility in this long loop may be a more general feature of the azurins. The two residues D76 and D77, which show increased T_1 values of 0.54 and 0.62 s, respectively, also have high *B*-factors in the *P. aeruginosa* crystal structure. These are the only regions for which the order parameters are reduced significantly. The presence of increased backbone mobility as inferred from the relaxation data is in this case also reflected in the crystallographic temperature factors. While the *B*-factor may increase by a

number of other processes than dynamics per se, the correspondence found suggests that the internal motions in question are still present when the molecules are arranged into a crystal lattice, in the case of *P. aeruginosa* azurin.

Conformational Exchange. The residues for which exchange contributions have been included in the order parameter fitting seem to cluster in the regions of the protein outside the β-strands (see Figure 3; the β-strands are indicated as solid bars on the abscissa). There are many amides with R_{ex} on the order of 1 Hz in the region between residues 53 and 79. This region comprises the flap region, consisting of the single α-helix and the loop between residues 67 and 79. Perhaps there is some motion on the micro- to millisecond time scale in the α-helix and adjacent loop region that slightly affects the T_2.

All residues but one displaying considerable exchange broadening (>2 Hz; residues 10, 11, 37, 45, and 88−90), are located in one part of the molecule. As seen in Figure 6, these residues surround the side chain of His-35. This suggests that the cause of the exchange broadening is a single conformational exchange effect involving the side chain of His-35. It has been shown that His-35 exhibits a deprotonation/protonation equilibrium that is slow on the chemical shift time scale. It has been argued in the Results section that the observed exchange broadening is caused by the His-35 deprotonation/protonation equilibrium. In the crystal structures at pH 5.5 and 9.0, a conformational difference is seen between the low- and high-pH structures. The residues that are most affected in the X-ray structures by the conformational rearrangement are Gly-37 and residues 9−12 and 88−91 from the two adjacent loops. From Figure 3, where the exchange contribution to T_2 is plotted against the residue number, it is seen that all these residues, with the exception of Gly-9, are among the ones that show exchange broadening in the present study. Residue Gly-45 has an exchange contribution of 9.5 Hz. This indicates that the peptide bond Met-44−Gly-45 is also influenced by the deprotonation of His-35, which is not surprising since the carbonyl of Met-44 is hydrogen-bonded to the $N^{\epsilon 2}$ of His-35.

Dynamic Conformational Changes in Redox Proteins. The ^{15}N backbone dynamics of azurin shows that the β-sheet scaffold of the protein, a feature that is shared with other type I blue copper proteins, produces an essentially rigid protein. The regions in which an increased mobility of the

backbone occurs on the pico- to nanosecond time scale are relatively far from the Cu site, and the loops that form the hydrophobic patch of azurin, which is the site where electron transfer takes place (*26*), do not show an increased mobility with respect to the core of the protein. Thus, the increased mobility in some parts of the backbone probably has no bearing on the electron-transfer function in azurin.

However, the protonation of His-35 affects the electron-transfer properties of azurin by changing the midpoint potential (*23*−*25*). Whether this phenomenon is of physiological relevance as a way to regulate azurin activity is difficult to judge, since the function of azurin has not yet been clearly established (*49*). Regulation of the midpoint potential by pH appears to occur in other blue copper proteins, like pseudoazurin, amicyanin, and plastocyanin, albeit via a different mechanism. In the reduced form of these proteins, the C-terminal, surface-exposed His ligand of the copper can be protonated, resulting in a change in copper coordination and a strong increase in the midpoint potential (*50*−*54*). Plastocyanin functions as an electron carrier in the lumen of thylakoids in photosynthetic electron transport. The pK_a for the protonation of the ligand His is around 5 (*55*). This suggests that the protonation could be a means of downregulation of plastocyanin activity, once a large protein gradient has been established over the thylakoid membrane and the pH in the lumen has dropped.

Recently, evidence was found that the protonation of the His ligand in amicyanin does not occur when amicyanin is bound to its redox partner methylamine dehydrogenase (*56*), thus causing a significant decrease in the midpoint potential of bound amicyanin at physiological pH. In this way, electrons can be transferred from the methylamine dehydrogenase−amicyanin complex to the redox partner cytochrome c_{551i}, while this is thermodynamically unfavorable for free amicyanin. In general, electron-transfer proteins are rigid, because rigidity results in a low reorganization energy and, therefore, in fast electron transfer. However, the present work, as well as the examples given above, demonstrates that electron-transfer proteins appear to have subtle switch mechanisms, based on dynamic conformational changes, to control their activity.

ACKNOWLEDGMENT

SUPPORTING INFORMATION AVAILABLE

Two tables containing the relaxation data, derived order parameters, τ_e, R_{ex}, and SSE values. This material is available free of charge via the Internet at http://pubs.acs.org.

REFERENCES

1. Nar, H., Messerschmidt, A., Huber, R., Van de Kamp, M., and Canters, G. W. (1991) *J. Mol. Biol. 221*, 765−772.
2. Adman, E. T., and Jensen, L. H. (1981) *Isr. J. Chem. 12*, 8−12.
3. Nar, H., Messerschmidt, A., Huber, R., Van de Kamp, M., and Canters, G. W. (1992) *FEBS Lett. 306*, 119−124.
4. Nar, H., Huber, R., Messerschmidt, A., Filippou, A. C., Barth, M., Jaquinod, M., Van de Kamp, M., and Canters, G. W. (1992) *Eur. J. Biochem. 205*, 1123−1129.
5. Moratal, J. M., Romero, A., Salgado, J., Perales-Alarcón, and Jiménez, H. R. (1995) *Eur. J. Biochem. 228*, 653−657.
6. Bonander, N., Vanngård, T., Tsai, L. C., Langer, V., Nar, H., and Sjölin, L. (1997) *Proteins: Struct., Funct., Genet. 27*, 385−394.
7. Nar, H., Messerschmidt, A., Huber, R., Van de Kamp, M., and Canters, G. W. (1991) *J. Mol. Biol. 218*, 427−447.
8. Sjölin, L., Tsai, L. C., Langer, V., Pascher, T., Karlsson, G., Nordling, M., and Nar, H. (1993) *Acta Crystallogr. D49*, 449−457.
9. Tsai, L. C., Sjölin, L., Langer, V., Pascher, T., and Nar, H. (1995) *Acta Crystallogr. D51*, 168−176.
10. Tsai, L. C., Sjölin, L., Langer, V., Bonander, N., Karlsson, G., Vänngård, T., Hammann, C., and Nar, H. (1995) *Acta Crystallogr. D51*, 711−717.
11. Tsai, L. C., Bonander, N., Harata, K., Karlsson, G., Vanngard, T., Langer, V., and Sjolin, L. (1996) *Acta Crystallogr. D: Biol. Crystallogr. 52* (Part 5), 950−958.
12. Hammann, C., Messerschmidt, A., Huber, R., Nar, H., Gilardi, G., and Canters, G. W. (1996) *J. Mol. Biol. 255*, 362−366.
13. Hammann, C., Van Pouderoyen, G., Nar, H., Gomis, R. F., Messerschmidt, A., Huber, R., den Blaauwen, T., and Canters, G. W. (1997) *J. Mol. Biol. 266*, 357−366.
14. Faham, S., Mizoguchi, T. J., Adman, E. T., Gray, H. B., Richards, J. H., and Rees, D. C. (1997) *J. Biol. Inorg. Chem. 2*, 464−469.
15. Karlsson, B. G., Tsai, L. C., Nar, H., Sanders-Loehr, J., Bonander, N., Langer, V., and Sjölin, L. (1997) *Biochemistry 36*, 4089−4095.
16. Messerschmidt, A., Prade, L., Kroes, S. J., Sanders-Loehr, J., Huber, R., and Canters, G. W. (1998) *Proc. Natl. Acad. Sci. U.S.A. 95*, 3443−3448.
17. Van de Kamp, M., Canters, G. W., Wijmenga, S. S., Lommen, A., Hilbers, C. W., Nar, H., Messerschmidt, A., and Huber, R. (1992) *Biochemistry 31*, 10194−10207.
18. Hoitink, C. W. G., Driscoll, P. C., Hill, H. A. O., and Canters, G. W. (1994) *Biochemistry 33*, 3560−3571.
19. Hill, H. A. O., Leer, J. C., Smith, B. E., Storm, C. B., and Ambler, R. P. (1976) *Biochem. Biophys. Res. Commun. 70*, 331−338.
20. Ugurbil, K., and Bersohn, R. (1977) *Biochemistry 16*, 3016−3023.
21. Hill, H. A. O., and Smith, B. E. (1979) *J. Inorg. Biochem. 11*, 79−93.
22. Canters, G. W., Hill, H. A. O., Kitchen, N. A., and Adman, E. T. (1984) *Eur. J. Biochem. 138*, 141−152.
23. Silvestrini, M. C., Brunori, M., Wilson, M. T., and Darley-Usmar, V. M. (1981) *J. Inorg. Biochem. 14*, 327−338.
24. Corin, A. F., Bersohn, R., and Cole, P. E. (1983) *Biochemistry 22*, 2032−2038.
25. Ugurbil, K., and Mitra, S. (1985) *Proc. Natl. Acad. Sci. U.S.A. 82*, 2039−2043.
26. Van de Kamp, M., Silvestrini, M. C., Brunori, M., Van Beeumen, J., Hali, F. C., and Canters, G. W. (1990) *Eur. J. Biochem. 194*, 109−118.
27. Van de Kamp, M., Canters, G. W., Andrew, C. R., Sanders-Loehr, J., Bender, C. J., and Peisach, J. (1993) *Eur. J. Biochem. 218*, 229−238.
28. Bashford, D., Karplus, M., and Canters, G. W. (1988) *J. Mol. Biol. 203*, 507−510.
29. Baker, E. N. (1988) *J. Mol. Biol. 203*, 1071−1095.
30. Lommen, A., and Canters, G. W. (1990) *J. Biol. Chem. 265*, 2768−2774.
31. Guss, J. M., Harrowell, P. R., Murata, M., Norris, V. A., and Freeman, H. C. (1986) *J. Mol. Biol. 192*, 361−387.
32. Barbato, G., Ikura, M., Kay, L. E., Pastor, R. W., and Bax, A. (1992) *Biochemistry 31*, 5269−5278.
33. Güntert, P., and Wüthrich, K. (1992) *J. Magn. Reson. 96*, 403−407.
34. Lipari, G., and Szabo, A. (1982) *J. Am. Chem. Soc. 104*, 4546−4559.

35. Lipari, G., and Szabo, A. (1982) *J. Am. Chem. Soc. 104*, 4559–4570.

36. Kay, L. E., Torchia, D. A., and Bax, A. (1989) *Biochemistry 28*, 8972–8979.

37. Clore, G. M., Driscoll, P., Wingfield, P. T., and Gronenborn, A. M. (1990) *Biochemistry 29*, 7378–7401.

38. Palmer, A. G., Hochstrasser, R. A., Millar, D. P., Rance, M., and Wright, P. E. (1991) *J. Am. Chem. Soc. 113*, 4371–4380.

39. Mandel, A. M., Akke, M., and Palmer, A. G. (1995) *J. Mol. Biol. 246*, 144–163.

40. Peng, J. W., and Wagner, G. (1992) *Biochemistry 31*, 8571–8586.

41. Kördel, J., Skelton, N. J., Akke, M., Palmer, A. G., and Chazin, W. J. (1992) *Biochemistry 31*, 4856–4866.

42. Smith, G. M., Yu, P. L., and Domingues, D. J. (1987) *Biochemistry 26*, 2202–2207.

43. Grzesiek, S., and Bax, A. (1993) *J. Am. Chem. Soc. 115*, 12593–12594.

44. Jeener, J., Meier, B. H., Bachmann, P., and Ernst, R. R. (1979) *J. Chem. Phys. 71*, 4546–4553.

45. Bloom, M., Reeves, L. W., and Wells, E. J. (1963) *J. Chem. Phys. 42*, 1615–1625.

46. Szyperski, T., Luginbühl, P. Otting, G., Güntert, P., and Wüthrich, K. (1993) *J. Biomol. NMR 3*, 151–164.

47. Orekhov, V. Y., Pervushin, K. V., and Arseniev, A. S. (1994) *Eur. J. Biochem. 219*, 887–896.

48. Nar, H. (1992) Ph.D. Thesis, Technische Universität München, Germany.

49. Vijgenboom E., Busch J. E., and Canters, G. W. (1997) *Microbiology (U.K.) 143*, 2853–2863.

50. Dennison, C., Kohzuma, T., McFarlane, W., Suzuki, S., and Sykes, A. G. (1994) *Inorg. Chem. 33*, 3299–3305.

51. Lommen, A., and Canters, G. W. (1990) *J. Biol. Chem. 265*, 2768–2774.

52. Katoh, S., Shiratori, I., and Takamiya, A. (1962) *J. Biochem. (Tokyo) 51*, 32–40.

53. Segal, M. G., and Sykes, A. G. (1978) *J. Am. Chem. Soc. 100*, 4585–4592.

54. DiBilio, A. J., Dennison, C., Gray, H. B., Ramirez, B. E., Sykes, A. G., and Winkler, J. R. (1998) *J. Am. Chem. Soc. 120*, 7551–7556.

55. Sykes, A. G. (1985) *Chem. Soc. Rev. 14,* 283–315.

56. Zhu, Z. Y., Cunane, L. M., Chen, Z. W., Durley, R. C. E., Mathews, F. S., and Davidson, V. L. (1998) *Biochemistry 37*, 17128–17136.

57. Cross, T. A., and Opella, S. J. (1983) *J. Am. Chem. Soc. 105*, 306–308.